Assessing Burn Severity Indexes for Fire Mapping using Multispectral Satellite Imagery

Lorenzo Carlassara

Politecnico di Milano, Geoinformatics Engineering

Abstract: Accurate burn severity assessment is crucial for understanding fire behavior, ecology, and post-fire management. While NASA Landsat satellites are commonly used, the newer European Space Agency Sentinel-2 satellites provide higher temporal and spatial resolution globally and free data access. Burn severity estimates was compared from Landsat and Sentinel in four different regions in western North America and South Europe affected by wildfires. Sentinel often outperforming Landsat, utilizing Sentinel's 20 m resolution reduced high-severity patch interior mapping compared to Landsat (30 m), indicating improved fine-scale fire effect detection. However, caution is advised when comparing severity patterns at different resolutions. Integrating Sentinel imagery enhances burn severity mapping by increasing availability and enabling finer-scale fire effect analysis. In the end, the accuracy assessment of the estimated burned area from Sentinel 2 was performed using the newly integrated QGIS plugin BAD (Burn Area Detector) as the ground truth.

The source code is available at the following GitHub repository

Key Words: Fire Mapping, Burn Severity, Spectral Indexes, Multispectral Images, Sentinel-2, Landsat 8, Google Earth Engine.

1. Introduction

Wildfires are natural phenomena with the potential for devastating consequences, leaving a trail of destruction in their wake. These catastrophic events pose significant challenges to ecosystems, human populations, and the environment. The damages caused by wildfires extend beyond the immediate destruction of vegetation and habitats; they have direct and long-term impacts on air quality, public health, property, and the ecological balance of affected areas. Although altered fire regimes have varied with complex ecological effects, human consequences are overwhelmingly negative, with impacts to human life and property, public health, culture, and economic systems(Syphard et al., 2022).

One of the most severe consequences of wildfires is the release of immense quantities of carbon dioxide and other greenhouse gases (GHGs) into the atmosphere. In California the GHG emissions from wildfires is the second most important source in the state (Jerrett et al., 2022). During the flaming phase of wildfires, carbon dioxide and nitrogen oxides are among the prominent emissions. Simultaneously, particulates, water vapor, and other compounds are expelled into the air, leading to compromised air quality. The smoldering phase, characterized by lower-intensity combustion, releases substances such as amines, ammonia, carbon monoxide, methane, and a spectrum of organics, each bearing its own ecological and environmental impact.

Among these complex interactions, the distinction between fire intensity and burn severity takes center stage. Fire intensity represents the energy released during various phases of a fire, and different metrics such as reaction intensity, fireline intensity, temperature, heating duration and radiant energy are useful for different purposes. Fire severity, and the related term burn severity, have created considerable confusion because of recent changes in their usage (Keeley, 2009). The observed effects often vary within the area and between different ecosystems. This includes alterations in soil properties, vegetation recovery, and hydrological regimes, all of which play pivotal roles in determining the long-term ecological health of a burned area. In Mediterranean-climate regions, accelerated erosion after wildfires can threaten ecosystem regeneration and natural capital recovery(Stefanidis et al., 2022). While fire intensity is indicative of the immediate fire behavior, burn severity provides insights into the lasting consequences of the fire on the landscape.

Advancements in remote sensing technology have enabled accurate and efficient assessment of burn severity using multispectral satellite imagery, with widespread use of Landsat imagery (Picotte et al., 2021) due to its global coverage, multi-decadal continuity, and open data policy beginning in 2008 (Woodcock et al., 2008). Recently, the addition of the Sentinel-2 constellation, to the network of Earth observation satellite missions brings new opportunities to improve burn severity mapping (Howe et al., 2022).

Sentinel, launched by the European Space Agency (ESA) in 2015 and 2017, comprises two platforms equipped with the same Multi-Spectral Instrument (MSI) sensor, designed to complement the Landsat mission, which is operated by the United States Geological Survey (USGS). However, it features notable distinctions that enhance its suitability for burn severity mapping. When compared to Landsat 8's, these differences include:

1. **Higher Spatial Resolution**: Sentinel offers finer spatial resolution for the bands used in dNBR and related indices (10 m NIR and 20 m SWIR), surpassing Landsat's 30 m.
2. **Increased Temporal Resolution**: The average revisit time of 3 to 5 days in the Sentinel constellation improves temporal resolution, contrasting Landsat's 16-day revisit cycle.
3. **Greater Spectral Resolution**: Sentinel incorporates 13 spectral bands, expanding the spectral resolution beyond Landsat's 9 bands.

The integration of advanced platforms like Google Earth Engine (GEE) further facilitates the processing and analysis of large-scale remote sensing data. This cloud-based geospatial analysis platform offers an array of tools to handle and process multispectral satellite imagery efficiently, allowing researchers

to conduct extensive analyses, generate accurate burn severity maps, and compare results between different datasets.

In pursuit of meticulous accuracy assessment, this investigation employs a Python-based accuracy assessment script within QGIS. This script, designed to evaluate the precision of burn severity mapping, assimilates random true points from a vector layer. These true points originate from the Burn Area Detector (BAD), a brand new QGIS plugin, which present itself with a practical graphical interface(Martinoli, 2023). The BAD plugin exemplifies the confluence of cutting-edge research and practical implementation, enriching the accuracy assessment process by supplying verifiable ground truth for evaluation.

2. Materials and method

The data utilized for this study were procured through a multifaceted approach, combining sources that encompass both global and regional wildfire monitoring systems. To establish a comprehensive foundation, the NASA Fire Information for Resource Management System (FIRMS), served as a primary data resource. FIRMS integrates data from diverse satellite platforms, including MODIS, Landsat, and NOAA, delivering a comprehensive view of wildfire occurrences and extents.

Complementing the global perspective, the European Forest Fire Information System of the European Commission's Joint Research Centre (EFFIS) and the European Emergency Management Service (EMS) provided more details. These platforms contributed spatially refined information on wildfire occurrences and progressions within Europe.

For a more localized perspective, we incorporated data from the California Department of Forestry and Fire Protection (CAL FIRE) which is renowned for its meticulous wildfire tracking and management. CAL FIRE furnished valuable insights into fire incidents and their ramifications in the California region.

The aggregation of data from these disparate sources allowed the construction of a robust and diverse dataset, encompassing global, regional, and local wildfire occurrences.

1. Rabbit Fire, Riverside county (California, USA) (CAL FIRE, 2023)
   14th July 2023 - 22nd July 2023

2. Mosquito Fire, Placer county (California, USA)(CAL FIRE, 2023)
   1st September 2022 - 20th September 2022

3. Rhodes wildfires (Dodecanese, Greece) (NASA Earth Observatory, 2023)
   18th July 2023 - 30th July 2023

4. Palermo wildfires (Sicily, Italy) (OpenDataSicilia, 2023)
   21st July 2023 - 9th August 2023

The identified fire incidents served as focal points for the analysis.

Data preprocessing of prefire and postfire multispectral images for the identified fire incidents consisted of a systematic approach, facilitated by GEE. This platform provided a centralized repository of up-to-date datasets, including those from FIRMS MODIS, Copernicus, Landsat, and administrative boundaries, ensuring the availability of comprehensive and contemporary information.

The initial step included the careful curation of the imagery data both from Sentinel-2 and from Landsat 8. To align the imagery with the scope of all the four incident areas, a precise spatial clipping procedure was implemented. This entailed constraining the Landsat 8 and Sentinel-2 collections to the geographic extents of each fire incident under investigation.

To ensure temporal alignment, further refinement was conducted by filtering the collection using defined temporal boundaries. The prefire dates were delineated using the `pre_date_start` and `pre_date_end`, whereas the postfire dates were identified using the `post_date_start` and `post_date_end` parameters. These constraints ensured the inclusion of imagery captured prior to and subsequent to the fire events.

Once the collection was curated and filtered, the median of the image stack was computed. This median composite encapsulated the central tendency of spectral information across the temporal range, minimizing the influence of transient atmospheric conditions or anomalies. The resultant median image formed the foundation for subsequent burn severity assessment, providing a representative snapshot of the prefire and postfire landscape for each incident.

The second phase of data preprocessing involved the precise handling of the datasets to ensure data integrity. To this end, a cloud masking function was implemented to eliminate cloud and cirrus cover within the Sentinel-2 imagery. This step safeguarded the accuracy of the subsequent analyses by reducing the influence of atmospheric artifacts.

Name	Description	Wavelength (nm)	Resolution
B1	Coastal Aerosol	0.433 - 0.453	30m
B2	Blue	0.450 - 0.515	30m
B3	Green	0.525 - 0.600	30m
B4	Red	0.630 - 0.680	30m
B5	NIR	0.845 - 0.885	30m
B6	SWIR 1	1.565 - 1.655	30m
B7	SWIR 2	2.105 - 2.285	30m
B8	Panchromatic	0.500 - 0.680	15m
B9	Cirrus	1.360 - 1.390	30m
B10	TIRS 1	1.070 - 1.110	100m
B11	TIRS 2	1.150 - 1.250	100m

Table 1. Landsat 8 Bands

Additionally, a function was developed to identify and mask water bodies present in the imagery and then remove them. The computation of the Normalized Difference Water Index (NDWI) with Landsat 8 images facilitated the detection of water-rich pixels, with higer Visible Green values and lower NIR values as shown in figure 1 (through Earth Observation for High Schools SEOS, 2023). These pixels were subsequently removed from the multispectral rasters.

Applying a NDWI (1) mask minimized potential confounding effects caused by water bodies, enhancing the reliability of burn severity assessments and for the further analysis in QGIS.

$$NDWI = \frac{B3 - B5}{B3 + B5} \tag{1}$$

The assessment of burn severity and its ecological consequences demanded the quantification of key spectral indices.

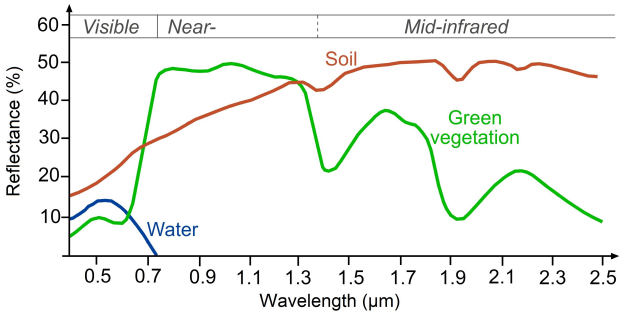

Figure 1. Spectral Signature

To this end, the Normalized Burn Ratio (NBR) and the differenced NBR (dNBR) (Howe et al., 2022) were crucial in detecting the extent of fire-induced alterations.

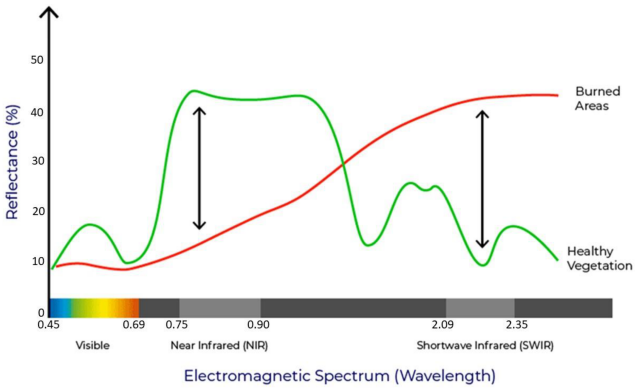

Figure 2. Burned Area Spectral Responses

For Landsat imagery, NBR (2) was calculated using the Near-Infrared (NIR) and Short-Wave Infrared (SWIR) bands, respectively B5 and B7 bands (1). On the other hand, for Sentinel-2, the NIR and SWIR bands are designated as Band 8A and Band 12 respectively (2) (ESA user guides, 2023). NBR embedded the contrast between live and burned vegetation.

$$NBR = \frac{NIR - SWIR}{NIR + SWIR} \tag{2}$$

Name	Description	Wavelength (nm)	Resolution
B1	Coastal Aerosol	443.9	60m
B2	Blue	459.7	10m
B3	Green	560	10m
B4	Red	664.5	10m
B5	Red Edge 1	703.9	20m
B6	Red Edge 2	740.2	20m
B7	Red Edge 3	782.5	20m
B8	NIR	835.1	10m
B8A	Narrow NIR	864.8	20m
B9	Water Vapor	945	60m
B10	SWIR - Cirrus	1375.0	60m
B11	SWIR 1	1613.7	20m
B12	SWIR 2	2202.4	20m

Table 2. Sentinel-2 Bands

To determine dNBR (3), post-fire and prefire NBR values were subtracted. Positive dNBR values indicate increased burn severity, while negative values denote post-fire recovery. This enabled a quantitative assessment of fire-induced changes.

$$dNBR = NBR_{prefire} - NBR_{postfire} \tag{3}$$

Furthermore, Burnt Area Index for Sentinel 2, BAIS2 [5], adapts the traditional BAI for Sentinel-2 bands, taking advantage of a combination of bands that have been demonstrated to be suitable for post-fire burned area detection (Visible (B4), Red-Edge (B6 and B7), NIR (B8A) and SWIR (B12) bands). The range of values for the BAIS2 is -1 to 1 for burn scars, and 1–6 for active fires(Alcaras et al., 2022). The BAIS2 index was so computed according to the following formula:

$$BAIS2 = (1 - \sqrt{\frac{B06 \cdot B07 \cdot B8A}{B4}}) \cdot (\frac{B12 - B8A}{\sqrt{B12 + B8A}} + 1) \tag{4}$$

The novelty introduced in the equation (4) for detecting fire affected areas is the use of a band ratio in the red-edge spectral domain, which aim to describe vegetation properties, combined with a band ratio to detect the radiometric response of the SWIR spectral domain, largely recognized to be efficient in the determination of burned areas ((Filipponi, 2018). This expression combined the spectral properties of the bands to capture the burn severity dynamics. BAIS2 encapsulated the interactions of vegetation, moisture content, and spectral responses, providing a holistic view of burn severity. The derivation of dBAIS2 (5) mirrored the process of dNBR, involving the subtraction of prefire BAIS2 from post-fire BAIS2. This transformation facilitated the assessment of spatial changes in burn severity, underscoring ecological transformations across the landscape.

$$dBAIS2 = BAIS2_{prefire} - BAIS2_{postfire} \tag{5}$$

The different distribution of BAIS2 compared to that of NBR leads to a different classification scale from the oned used by EMS (3), which has to be adapted when displaying the grading levels. Due to a slight difference in wavelengths (2) and (2), the same can also be said of Landsat's NBR compared to Sentinel's, however in this case the difference is minimal and therefore will be neglected.

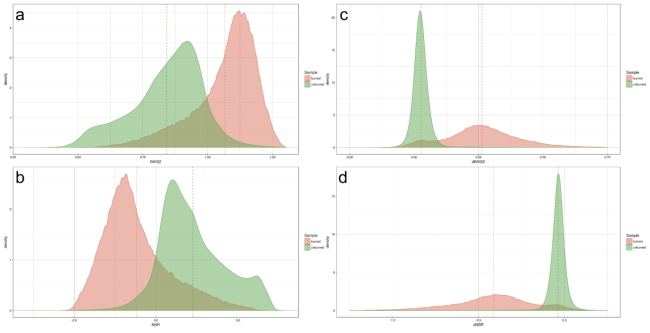

Figure 3. (a) Distribution of burned and unburned pixels values for BAIS2 index; (b) Distribution of burned and unburned pixels values for NBR index; (c) Distribution of burned and unburned pixels values for dBAIS2 index; (d) Distribution of burned and unburned pixels values for dNBR index

The quantification of burned area enabled a comprehensive understanding of fire extent and its ecological ramifications. To

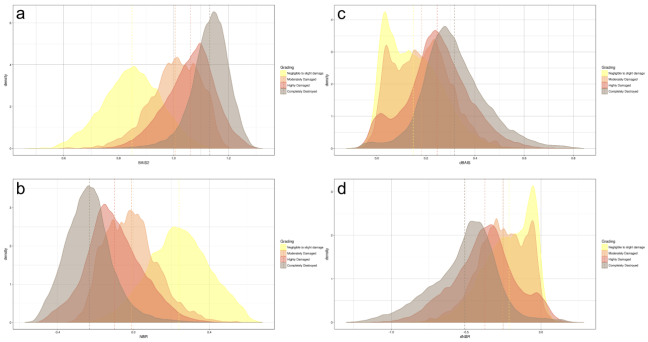

Figure 4. (a) Distribution of pixels values for BAIS2 index with respect to the EMS grading levels; (b) Distribution of pixels values for NBR index with respect to the EMS grading levels; (c) Distribution of pixels values for dBAIS2 index with respect to the EMS grading levels; (d) Distribution of pixels values for dNBR index with respect to the EMS grading levels

achieve this, we employed the differenced Normalized Burn Ratio (dNBR) as a critical threshold for identifying and extracting burned pixels(UN-SPIDER, 2023).

The selection criterion for identifying burned pixels was based on a threshold value of dNBR greater than or equal to 100. This threshold effectively pointed areas with high burn severity, indicative of significant fire-induced alterations.

Having isolated the burned pixels, our analysis transitioned to computing the area represented by each of these pixels. To this end, the area of individual pixels was calculated using the correct spatial geometry and scale. Subsequently, the cumulative sum of the areas of the burned pixels was derived through the application of a 'reduce region' operation, effectively aggregating the individual pixel areas within the specified geographic scope.

The resulting cumulative area was initially expressed in square meters. To provide a more intuitive representation, the area was subsequently converted to hectares and acres. The conversion involved dividing the area in square meters by 10,000 to obtain hectares, and by 4,046.86 to obtain acres.

In our pursuit of accurate burn severity assessment, we switched to QGIS, employing the Burn Area Detector (BAD) plugin. This step enabled us to compute burn severity, ensuring robust accuracy assessment.

To initiate this process, the prefire and postfire images, with all the Sentinel-2 bands, were exported from GEE. These images served as the foundation for computing burn severity through the BAD plugin. With the prefire and postfire imagery at our disposal, the BAD plugin facilitated the computation of burn severity.

Subsequently, the previously computed dNBR results from Sentile-2 were compared with the outcomes of the Region Growing algorithm from BAD. The latter entailed delineating burned areas based on distinctive spectral signatures indicative of burn severity. The comparison of these two burn severity assessment methodologies—dNBR and Region Growing—formed the crucial point of the accuracy assessment.

Finally, a comparison between the results of dNBR against a set of randomly selected true points, obtained from the BAD plugin Region Growing quantified the accuracy of the burn severity assessment.

3. Results discussion

This study sheds light on how severe fires are and how we can measure that. The variety of tools deployed, like GEE, the BAD plugin, and QGIS helps to understand wildfires better. Furthermore the GEE script was adapted to a python notebook to make the project more accessible and editable.

In GEE, we looked at the severity of the burn using different grading levels. Due to a minor variance in wavelengths (as shown in Table 1 and 2), a similar observation can also be made regarding the comparison between Landsat's and Sentinel's NBR. Nonetheless, this discrepancy is negligible and thus is disregarded. We also saw that the area burned in some fires was different from what official sources like CAL FIRE and the Greek Reporter(Kokkinidis, 2023) said. The slight difference, always greater in the declared burned area, could mean that it's tough to quickly estimate how much a fire has burned, rather than a discrepancy in the script computation.

Incident Region	estimate (LS8)		declared	
	hectares	acres	hectares	acres
Rabbit Fire	3291	8133	-	8283
Mosquito Fire	20429	50480	-	76788
Rhodes	17535	43329	13500	-
Palermo	10106	24973	-	-

Table 3. Burned Areas Comparison

Two satellite types were also compared: Landsat and Sentinel-2. Landsat has a lower picture quality, so it often showed more area burned compared to Sentinel-2. This was what we expected because Landsat can't see small details as well.

In QGIS, we checked how accurate our burn severity estimates were. Our results showed that our method worked well. We used a special script to make a confusion matrix, which helped us see how accurate our estimates were. The BAD plugin, made by CNR, also helped us make our estimates more reliable by giving us accurate information.

Burned Area	0 (PP)	1 (PN)	UA	PA	OA
0 (P)	979	178	0.85	0.98	0.901
1 (N)	21	822	0.98	0.82	

Table 4. Mosquito Fire, California USA 2022 - Confusion Matrix

Burned Area	0 (PP)	1 (PN)	UA	PA	OA
0 (P)	482	58	0.89	0.96	0.924
1 (N)	18	442	0.96	0.88	

Table 5. Rabbit Fire, California USA 2023 - Confusion Matrix

But we faced some challenges. For example, in the Palermo wildfires (7), it was hard to know exactly how much was burned. Wildfires are complex, and this incident showed that figuring out the burned area can be tricky because of the environment, the landscape, and how we measure it.

In the end, our study shows that measuring burn severity is challenging task. Using tools like GEE, the BAD plugin, and QGIS, we got a better picture of how fires affect the environment. As we continue to learn about wildfires and how to manage them, our findings will help us make better decisions to protect nature and recover from these events.

Burned Area	0 (PP)	1 (PN)	UA	PA	OA
0 (P)	498	11	0.98	1.0	0.987
1 (N)	18	442	1.0	0.98	

Table 6. Rhodes Wildfires, Greece 2023 - Confusion Matrix

Burned Area	0 (PP)	1 (PN)	UA	PA	OA
0 (P)	475	147	0.76	0.96	0.828
1 (N)	25	353	0.93	0.71	

Table 7. Palermo Wildfires, Italy 2023 - Confusion Matrix

References

Alcaras, E., Costantino, D., Guastaferro, F., Parente, C., Pepe, M., 2022. Normalized Burn Ratio Plus (NBR+): A New Index for Sentinel-2 Imagery. *MDPI Journal, remote sensing*. https://doi.org/10.3390/rs14071727.

CAL FIRE, 2023. Incident archive.

ESA user guides, 2023. Sentinel-2 msi spatial resolutions. Online. `https://sentinels.copernicus.eu/web/sentinel/user-guides/sentinel-2-msi/resolutions/spatial`.

Filipponi, F., 2018. BAIS2: Burned Area Index for Sentinel-2. *MDPI Journal*. doi:10.3390/ecrs-2-05177.

Howe, A. A., Parks, S. A., Harvey, B. J., Saberi, S. J., Lutz, J. A., Yocom, L. L., 2022. Comparing Sentinel-2 and Landsat 8 for Burn Severity Mapping in Western North America. *MDPI Journal, remote sensing*. https://doi.org/10.3390/rs14205249.

Jerrett, M., Jina, A. S., Marlier, M. E., 2022. Up in smoke: California's greenhouse gas reductions could be wiped out by 2020 wildfires. *Environmental Pollution*. www.elsevier.com/locate/envpol.

Keeley, J. E., 2009. Fire intensity, fire severity and burn severity: a brief review and suggested usage. *International Journal of Wildland Fire*, 116–126. https://doi.org/10.1071/WF07049.

Kokkinidis, T., 2023. Fires on rhodes, greece burned 13,500 hectares of forest. Online. `https://greekreporter.com/2023/08/01/fires-rhodes-greece-burned-13500-hectares-forest/`.

Martinoli, T., 2023. Burned area detector: development of a QGIS plugin for mapping burned areas from Sentinel-2 images. Geoinformatics Engineering Master Degree Thesis, Politecnico di Milano - CNR-IREA.

NASA Earth Observatory, 2023. Fires ignite on greek islands. Online. `https://earthobservatory.nasa.gov/images/151628/fires-ignite-on-greek-islands`.

OpenDataSicilia, 2023. Palermo hub. Online. `http://palermohub.opendatasicilia.it/monreale.html#12/38.1325/13.4121`.

Picotte, J. J., Cansler, C. A., Kolden, C. A., Lutz, J. A., Key, C., Benson, N. C., Robertson, K. M., 2021. Determination of burn severity models ranging from regional to national scales for the conterminous United States. *Remote Sensing of Environment*. https://doi.org/10.1016/j.rse.2021.112569.

Stefanidis, S., Alexandridis, V., Spalevic, V., Mincato, R. L., 2022. Willdfire Effects on Soil Erosion Dynamics: The Case of 2021 Megafires in Greece. *Agriculture Forestry, Vol. 68*, 49—63. DOI: 10.17707/AgricultForest.68.2.04.

Syphard, A. D., Keeley, J. E., Gough, M., Lazarz, M., Rogan, J., 2022. What MakesWildfires Destructive in California? *MDPI Journal*. https://doi.org/10.3390/fire5050133.

through Earth Observation for High Schools SEOS, S. E., 2023. Introduction to categorisation of objects from their data.

UN-SPIDER, 2023. Office for outer space affairs un-spider knowledge portal. normalized burn ratio (nbr). Online. `https://un-spider.org/advisory-support/recommended-practices/recommended-practice-burn-severity/in-detail/normalized-burn-ratio`.

Woodcock, C. E., Allen, R., Anderson, M., Belward, A., Bindschadler, R., Cohen, W., Gao, F., Goward, S. N., Helder, D., Helmer, E., Nemani, R., Oreopoulos, L., Schott, J., Thenkabail, P. S., Vermote, E. F., Vogelmann, J., Wulder, M. A., Wynne, R., 2008. DOI: 10.1126/science.320.5879.1011a.